Quantitative evaluation of fabrication processes of proton-exchanged layers in LiTaO3 optoelectronic devices by the line-focus-beam ultrasonic material characterization system

doi: 10.1063/1.1340008

Quantitative evaluation of fabrication processes of proton-exchanged layers in $LiTaO_3$ optoelectronic devices by the line-focus-beam ultrasonic material characterization system

J. Kushibiki[a] and M. Miyashita
Department of Electrical Engineering, Tohoku University, Sendai 980-8579, Japan

(Received 3 July 2000; accepted for publication 16 November 2000)

Experimental investigations are conducted in order to collect basic data for evaluating proton-exchanged $LiTaO_3$ optical waveguides and their fabrication processes and systems using the line-focus-beam ultrasonic material characterization system, in the frequency range 100–300 MHz. Seven *Z*-cut $LiTaO_3$ substrates are proton exchanged at several process temperatures (220–280 °C) and times (5–30 min) in a pyrophosphoric acid solution. Leaky surface acoustic wave (LSAW) velocities, measured for all specimens, decrease for all propagation directions. The decrease rate is at maximum in the *Y*-axis propagation direction, in which the measurement sensitivity to the process conditions is highest. The fH dependences of LSAW velocities, obtained from frequency dependences of LSAW velocities and proton-exchanged layer depths analyzed by secondary-ion mass spectrometry, have almost constant gradients of -0.78 (m/s)/(Hz m). Normalized depth distributions of the elastic properties of proton-exchanged layers are nearly equal; only the depths differ. Also, the relationships among LSAW velocities, layer depths, process times, process temperatures, and diffusion coefficients are experimentally obtained. Homogeneity evaluation of a proton-exchanged, 2-in., *Z*-cut $LiTaO_3$ wafer processed at 260 °C for 14 min is demonstrated, resulting in a maximum LSAW velocity variation of 1.3 m/s. This corresponds to a depth variation of 7.4 nm and a temperature variation of 0.8 °C for the whole surface. © *2001 American Institute of Physics.* [DOI: 10.1063/1.1340008]

I. INTRODUCTION

Research studies and developments of various waveguide-type optoelectronic devices, such as modulators and demodulators,[1] switches,[2] filters,[3] and optical sources of short wavelengths,[4–7] have been conducted in order to meet the increasing demands of high-capacity, high-speed telecommunications of recent years, using $LiNbO_3$ and $LiTaO_3$ single crystals for their advantages, such as electro-optic, acousto-optic, and optical nonlinear effects. The performance characteristics of the waveguide-type optoelectronic devices constructed are considered to depend mainly upon the following three factors: (1) homogeneity of crystallographic, physical, chemical, and optical properties of materials, (2) machining and polishing damage on the wafer surfaces, and (3) uniformity of device fabrication processes. The proton-exchange method[6] without and with annealing is widely used in fabricating waveguide-type optoelectronic devices to produce optical waveguides on $LiNbO_3$, $MgO:LiNbO_3$, and $LiTaO_3$ single-crystal substrates. Furthermore, proton exchange followed by heat treatment[7] is used as a method to form domain inversion layers on $LiTaO_3$ crystal substrates. Conventionally, secondary-ion mass spectrometry (SIMS) has been applied to evaluate proton-exchanged optical waveguides to determine the depths and atom distributions,[8] and the prism coupler method,[9,10] to determine the depths and refractive index profiles.[6,11] A very important subject for future practical use of the optical devices is to develop optimal fabrication processes and systems for mass production using large-diameter crystal wafers. The fabrication processes and systems must, therefore, be evaluated and improved by feeding back the evaluation results. However, there are some serious problems with the SIMS and prism coupler methods. The former is destructive and lacks quantitativeness, and the latter cannot be applied to single-mode optical waveguides. It is, therefore, necessary to develop a new technique capable of nondestructive, quantitative measurement with high accuracy, as well as to improve these conventional means.

We have proposed line-focus-beam (LFB) acoustic microscopy[12] as a new technique applicable to these evaluations. LFB acoustic microscopy is a technology to quantitatively evaluate and analyze elastic properties of materials by measuring propagation characteristics (phase velocity and propagation attenuation) of leaky surface acoustic waves (LSAWs) propagating on the water-loaded specimen surface with high accuracy. The system has been successfully applied to characterize optical-grade $LiNbO_3$, $MgO:LiNbO_3$, and $LiTaO_3$ single crystals. We have also sought to establish single-crystal growth conditions to grow homogeneous, large-diameter single crystals by investigating the relationships among the LSAW velocities, densities, chemical composition ratios, and lattice constants.[13,14] This ultrasonic system is also considered to be a very useful tool for evaluating and analyzing layered specimens such as thin films and diffused or implanted layers, as this technique employs the

[a]Electronic mail: kushi@ecei.tohoku.ac.jp

mode of surface acoustic waves for characterization.[12,15–20] The LFB system has been demonstrated to characterize proton-exchanged, *Z*-cut $LiNbO_3$ and $LiTaO_3$ optical waveguides. It has also been shown that LSAW velocities decrease depending on process conditions, essentially the process temperature and time, and that the system sensitivity to the depth changes of proton-exchanged layers surpasses the sensitivity of any conventional method.[16] Furthermore, the LFB system has successfully characterized domain-inverted layers in *Z*-cut $LiTaO_3$ single-crystal substrates by comparing the measured LSAW velocities with the theoretical results.[17,18] There also have been reports on the propagation characteristics of LSAWs measured on proton-exchanged *X*-, *Y*- and *Z*-cut $LiNbO_3$ substrates[19] and on LSAW velocities measured on proton-exchanged *Z*-cut $LiTaO_3$ and proton-exchanged and annealed $LiTaO_3$.[20] The measurement results reported have shown the possibilities of evaluating proton-exchanged optical waveguides and their fabrication processes and systems by the LFB acoustic microscopy system.

The purpose of this article is to obtain basic data on the relationship between LSAW velocities and proton-exchange fabrication process conditions using pyrophosphoric acid. The data could then be used as a dictionary to interpret results obtained by the LFB system, and to demonstrate the usefulness for characterizing proton-exchanged optical waveguides and their fabrication processes. Here, the process temperature and time are taken as parameters of the fabrication process conditions. Several specimens of proton-exchanged *Z*-cut $LiTaO_3$ substrates are fabricated under several different conditions. LSAW velocities of these specimens are measured by LFB acoustic microscopy, depth profiles of proton and lithium ions are analyzed by SIMS, and the depths of proton-exchanged layers are measured.

II. LFB SYSTEM

The most recent LFB ultrasonic material characterization (UMC) system[21] is used to measure $V(z)$ curves. Elastic properties of materials are characterized by obtaining the propagation characteristics of LSAWs, viz., phase velocity and propagation attenuation, from the $V(z)$ curve, which is the transducer output of LSAWs excited and propagating on a water-loaded specimen surface when the relative distance z between an ultrasonic LFB device and the specimen is varied.[12] The LSAW velocities are employed for material characterization here. Figure 1 shows a typical $V(z)$ curve measured for a *Z*-cut $LiTaO_3$ substrate in the *Y*-axis propagation direction and its spectral distribution, obtained through fast Fourier transform (FFT) analysis. According to the analytical procedure of $V(z)$ curves, the LSAW velocity is determined from the following equation:

$$V_{\mathrm{LSAW}}=\frac{V_w}{\sqrt{1-(1-(V_w/2f\cdot\Delta z))^2}}, \tag{1}$$

where Δz is the oscillation interval in the $V(z)$ curve, V_w is the longitudinal velocity in water, and f is the ultrasonic frequency. When the LFB system is applied to characterize thin specimens such as wafer-type substrates 0.3–1.0 mm thick,

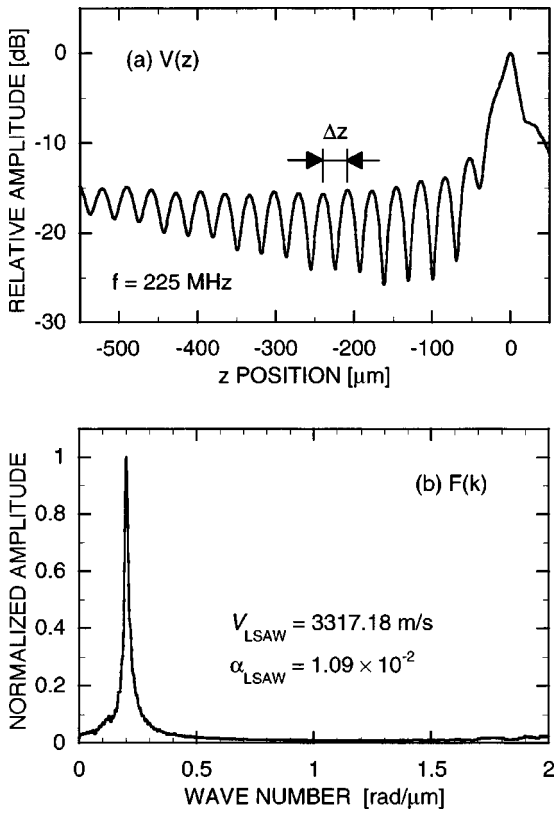

FIG. 1. Typical $V(z)$ curve measured for *Z*-cut, *Y*-propagating $LiTaO_3$ at 225 MHz (a) and spectral distributions analyzed by FFT for the $V(z)$ curve shown above (b).

we have to consider the measurement errors due to the influence of the waves reflected from the back surface of the specimen.[22] To resolve this problem, a useful method of moving-average processing of the frequency dependence of LSAW velocities at each measurement position and an approximated correction method, which is very useful for a great number of measurements, have been developed.[22,23] Here, LSAW velocity variations caused by the proton exchange can be obtained approximately by taking the differences between two velocities measured at the same frequency at the same measurement point on the specimen before and after proton exchange.

III. PREPARATION OF SPECIMENS

Specimens with proton-exchanged layers were prepared using a fabrication system consisting of a temperature controllable aluminum (Al) dry block bath system (Scinics Co., Ltd., Tokyo, Japan), a sample transportation system, a temperature measurement system, and a computer for controlling sample transportation and temperature measurement. Beakers with capacities of 200, 300, or 500 cm^3 can be placed in the corresponding furnace holes of the dry block bath, and a liquid solution of pyrophosphoric acid contained in each beaker can be heated uniformly. Substrates were 0.5-mm-thick, *Z*-cut $LiTaO_3$ wafers (optical grade, Yamaju Ceramics Co., Ltd., Seto, Japan) and were processed in a 200-cm^3 SiO_2 glass beaker. Figure 2 illustrates the sample preparation procedure. Each specimen is a quarter piece of a

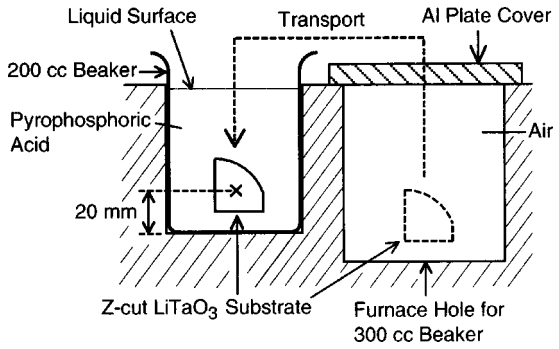

FIG. 2. Sample preparation.

TABLE I. Fabrication conditions and parameters for proton-exchanged, *Z*-cut $LiTaO_3$ specimens.

Sample No.	Process conditions: Temperature [°C]	Process conditions: Time [min]	Depth of proton-exchanged layer [μm]	Diffusion coefficient [$\mu m^2/h$]
1	260.3	5	0.243	0.176
2	259.9	14	0.411	0.176
3	260.1	20	0.465	0.176
4	260.0	30	0.603	0.176
5	220.2	14	0.160	0.027
6	239.7	14	0.248	0.066
7	280.8	14	0.638	0.436

2-in. $LiTaO_3$ substrate. A specimen is set on a sample holder made of SiO_2 glass and then placed in the furnace hole for a 300-cm^3 beaker in the Al dry block bath to preheat the specimen to the temperature for the proton-exchange process. A beaker containing approximately 380 g (200 cm^3) of an undiluted solution of pyrophosphoric acid (concentration exceeding 93%, Kanto Chemical Co., Inc., Tokyo, Japan) is set in the 200-cm^3-beaker furnace hole. The beaker, pyrophosphoric acid solution, $LiTaO_3$ substrate, and sample holder are simultaneously heated through the Al dry block bath with the heater built in. They are kept heated until the temperature of the pyrophosphoric acid solution, which is monitored by a thermocouple sealed in a small SiO_2 glass tube, reaches the desired temperature and sufficiently stabilizes (within 0.4 °C). The $LiTaO_3$ substrate set on the sample holder is then transferred by the transportation system into the beaker with the pyrophosphoric acid solution and undergoes proton exchange. The specimen is placed at the center of the beaker about 20 mm above the bottom, where the temperature distribution of the pyrophosphoric acid solution is nearly uniform. After the required time period, the $LiTaO_3$ substrate and sample holder are pulled out, cooled naturally, and rinsed with pure water to remove residual pyrophosphoric acid.

The depth of the proton-exchanged layer H depends on the proton-exchange process time t and the diffusion coefficient $D(T)$ and is expressed as follows:[6,11]

$$H = 2\sqrt{t \cdot D(T)}, \tag{2}$$

where T is the temperature of the proton-exchange process. And the diffusion coefficient $D(T)$ is related as

$$D(T) = D_0 \exp\left(-\frac{Q}{RT}\right), \tag{3}$$

where D_0 is the diffusion constant, Q is the activation energy, and R is the universal gas constant. Thus the process time and process temperature are chosen here as the proton-exchange process conditions. Following the experimental procedure described above, seven proton-exchanged specimens were prepared using process times and temperatures shown in Table I. These parameters were chosen in accordance with the process conditions for fabricating optical waveguides of second harmonic generation (SHG) devices (for 14 min at 260 °C) and for fabricating periodically domain-inverted layers by proton exchange and heat treatment to form quasiphase matching (QPM)[24] (for 20 min at 260 °C).[25] A new material of pyrophosphoric acid as the proton source is used to prepare each specimen.

IV. EXPERIMENTS

A. Angular dependences

To investigate the relationship between the process conditions and elastic property changes caused by proton exchange, angular dependences of LSAW velocities were measured near the center of the negative Z surface of each specimen in 1° steps before and after the proton exchange. The ultrasonic frequency was set at 225 MHz. Figures 3(a) and 3(b) give the measured results for specimen Nos. 1–4, which were prepared at a fixed temperature of 260 °C with process time varied, and for specimen Nos. 2 and 5–7, prepared for a fixed period of 14 min with process temperature varied. The crystallographic X axis and Y axis correspond to 0° and 90° in the figures, respectively. For each specimen, the proton exchange causes the LSAW velocities to decrease in all the propagation directions, and the LSAW velocities decrease as the process time and temperature increase, as seen in Figs. 3(a) and 3(b). The LSAW velocities exhibit symmetrical cycles of 60°, reflecting the crystallographic symmetry of a *Z*-cut $LiTaO_3$ single crystal. However, as the process time or the process temperature increases, the differences between the relative maxima and minima decrease. These changes in elastic properties are induced by the proton exchange because the acoustical physical constants (elastic constant, piezoelectric constant, dielectric constant, and density) of proton-exchanged layers differ from those of the substrates, and proton-exchanged layers have the elastic property of lower LSAW velocities as reported on $LiNbO_3$ and $LiTaO_3$.[26,27] The LSAW velocity changes are 35.7–48.6 m/s for specimen No. 1, 59.1–78.3 m/s for specimen No. 2, 69.0–90.8 m/s for specimen No. 3, and 84.2 to 110.0 m/s for specimen No. 4 in Fig. 3(a), and 23.0–31.8 m/s for specimen No. 5, 37.0–50.1 m/s for specimen No. 6, and 88.3–114.9 m/s for specimen No. 7 in Fig. 3(b). The LSAW velocity changes were observed to be the largest in the Y-axis propagation direction and the smallest in the X-axis direction for both sets of specimens prepared with either the process time or temperature varied. Therefore we conclude that the Y-axis propagation direction is the best choice for evaluating proton-exchanged layers and their process conditions on

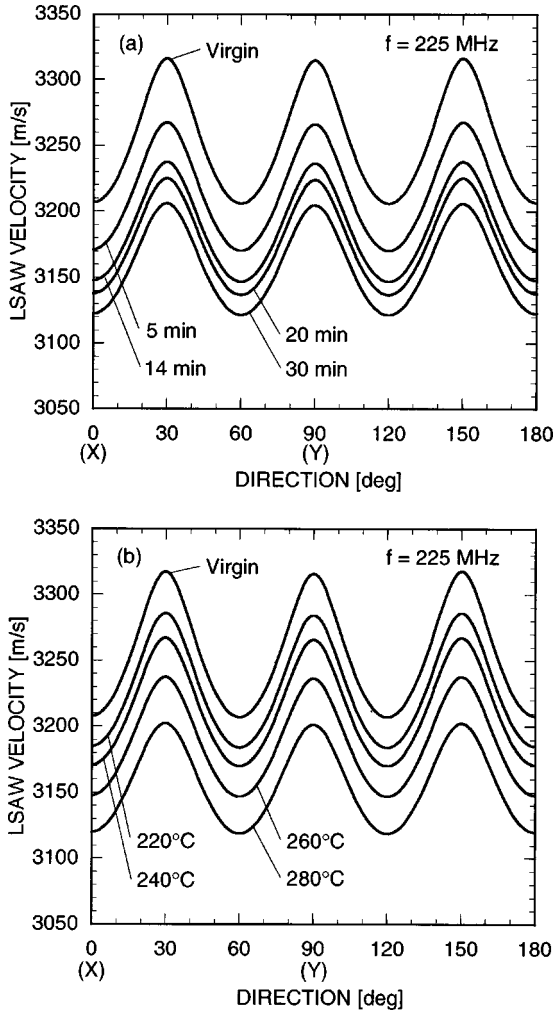

FIG. 3. Angular dependences of LSAW velocities for proton-exchanged, *Z*-cut $LiTaO_3$ specimens. (a) Results for the specimens processed for 5, 14, 20, and 30 min at 260 °C. (b) Results for the specimens processed at 220, 240, 260, and 280 °C for 14 min.

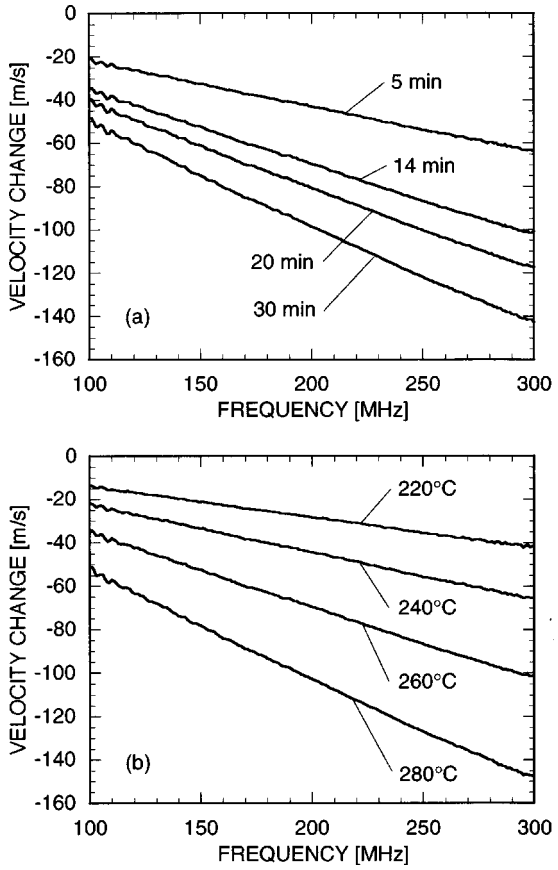

FIG. 4. Frequency dependences of LSAW velocities for proton-exchanged, *Z*-cut $LiTaO_3$ specimens. (a) Results for the specimens processed for 5, 14, 20, and 30 min at 260 °C. (b) Results for the specimens processed at 220, 240, 260, and 280 °C for 14 min.

Z-cut $LiTaO_3$ substrates by the LFB system, since it is most sensitive to changes of the process conditions.

B. Frequency dependences

In general, propagation characteristics of LSAW velocities in layered media are dispersive,[12,15] so LSAW velocities were measured near the center of the negative *Z* surface of each specimen in 1-MHz steps from 100 to 300 MHz for the *Y*-axis propagation before and after the proton exchange. Figure 4 shows the frequency dependences of LSAW velocity changes extracted by taking the differences between the velocities measured before and after the proton exchange. Figure 4(a) is for specimen Nos. 1–4, and Fig. 4(b) is for specimen Nos. 2 and 5–7. In each specimen, the LSAW velocities decrease nearly linearly as the frequency increases. Since the depths of the proton-exchanged layers formed on the specimens increase as the process time or temperature increases, the LSAW velocity decreases more distinctly, exhibiting a steeper slope and presumably more strongly reflecting the elastic properties of the proton-exchanged layers.

C. Hydrogen and lithium profiles

Profiles of hydrogen and lithium as a function of distance from the surface were analyzed by the SIMS method to examine the depths of the proton-exchanged layers formed on the specimen surfaces. The results are shown in Fig. 5(a) for specimen Nos. 1–4 and in Fig. 5(b) for specimen Nos. 2 and 5–7. In the ordinate of the figures, secondary-ion intensities of hydrogen were normalized by the intensities at the surface position as the surface intensities for all specimens were almost the same within the measurement errors, while those of lithium were normalized by the intensities in the bulk substrate region. In every specimen, the proton exchange causes hydrogen to diffuse into the substrate and to distribute over some distances to the boundary between the proton-exchanged layer and the bulk substrate, and its secondary-ion intensity gradually decreases as the distance increases. Around the boundary, the hydrogen intensity decreases abruptly as the distance increases further. Lithium's secondary-ion intensity exhibits an abrupt increase around the boundary and saturates to the value of the bulk substrate as the distance increases further. The position at which the secondary-ion intensity of hydrogen reaches $1/e$ of the surface intensity is determined as the depth of the proton-exchanged layer, and the results are listed in Table I. Errors in the determined depths of the proton-exchanged layers are given by the sum of the depth measurement errors by the

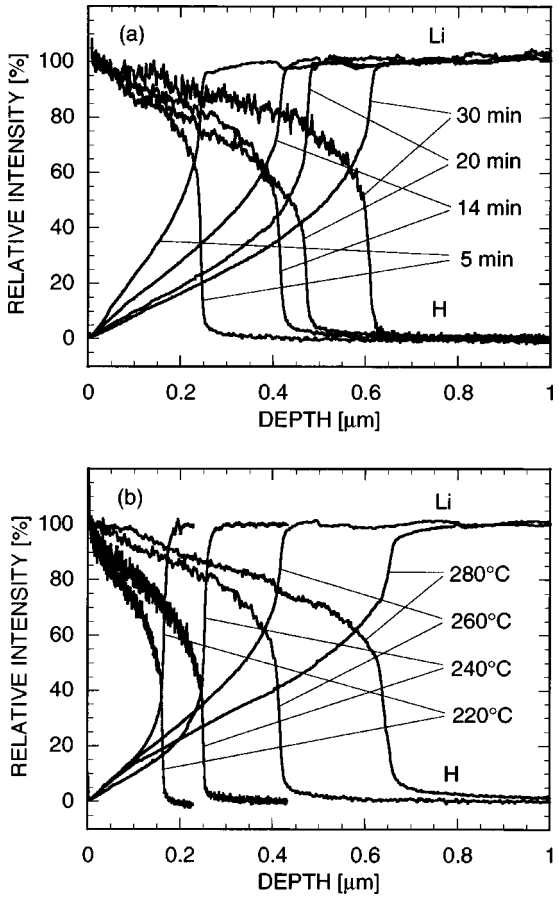

FIG. 5. H and Li depth profiles for proton-exchanged, *Z*-cut $LiTaO_3$ specimens analyzed by secondary-ion mass spectrometry. (a) Results for the specimens processed for 5, 14, 20, and 30 min at 260 °C. (b) Results for the specimens processed at 220, 240, 260, and 280 °C for 14 min.

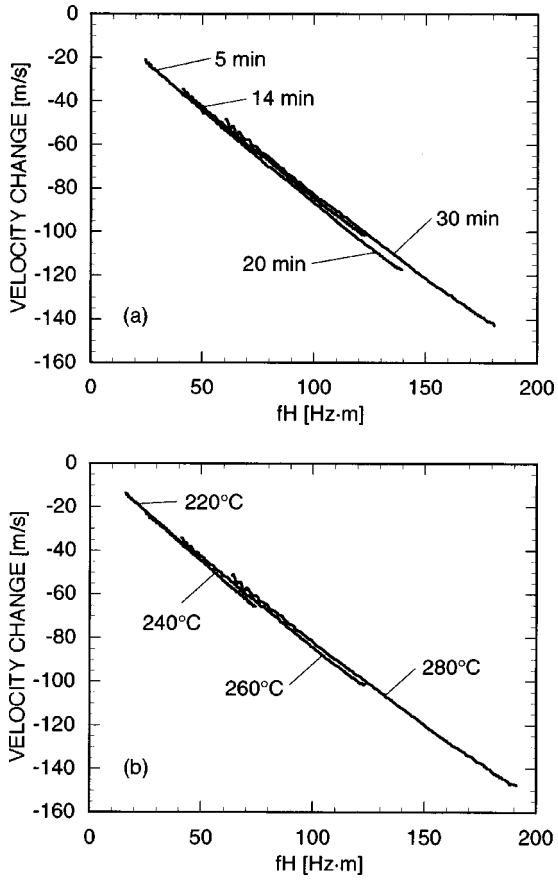

FIG. 6. fH dependences of LSAW velocities for proton-exchanged, *Z*-cut $LiTaO_3$ specimens. (a) Results for the specimens processed for 5, 14, 20, and 30 min at 260 °C. (b) Results for the specimens processed at 220, 240, 260, and 280 °C for 14 min.

stylus profiler system (Dektak 3ST, Veeco Instruments Inc., New York) and the depth resolution by the SIMS system (PHI SIMS 6600, Physical Electronics, Inc., Minnesota), and are estimated to be ± 0.03 μm. As the proton-exchange process time or the process temperature increases, hydrogen ions diffuse into the substrate as lithium ions are transported from the deeper area of the substrate toward the surface and diffuse out from the substrate surface, thus decreasing the intensity at the surface and forming a deeper proton layer. The proton-exchanged layer depths thus clearly depend on the process conditions. The diffusion coefficients given by Eq. (2) are also listed in Table I.

V. DISCUSSIONS

A. *fH* dependences

fH dependences of the LSAW velocities were obtained using the proton-exchanged layer depths in Table I and the frequency dependences shown in Fig. 4. Figure 6(a) shows the fH dependences of the LSAW velocity changes for specimen Nos. 1–4, and Fig. 6(b) for specimen Nos. 2 and 5–7. For all the specimens, the LSAW velocities decrease linearly with their fH having nearly equal gradients and overlapping each other. The gradients of the approximated lines obtained for the results of the fH dependences in Figs. 6(a) and 6(b) by the least-squares method are -0.789 and -0.774 (m/s)/(Hz m), respectively, in the measured region.

In general, the propagation characteristics of Rayleigh-type LSAWs, the fundamental propagation mode, strongly reflect the elastic properties of the specimen within one wavelength beneath the surface. Consequently, as f or H increases, the propagation characteristics of LSAWs decrease more significantly because they more strongly reflect the less elastic properties of the proton-exchanged layers than those of the substrates.[16] Therefore the fact that the fH dependences obtained for each specimen resulted in a single line by overlapping each other indicates that depth distributions of the elastic characteristics in the proton-exchanged layers normalized by the layer depths are equivalent, although there are obvious differences in H. This also corresponds to the fact that the H and Li profiles as a function of normalized depth obtained from Fig. 5 are almost the same for all specimens and that only the layer depths are different. We can take a simple measurement model of a single-layered specimen with a step-like elastic property change, and can estimate the proton-exchange process condition changes and depth changes in the measured region from the specific gradient value of -0.78 (m/s)/(Hz m) in the fH dependence of LSAW velocities for pyrophosphoric acid.

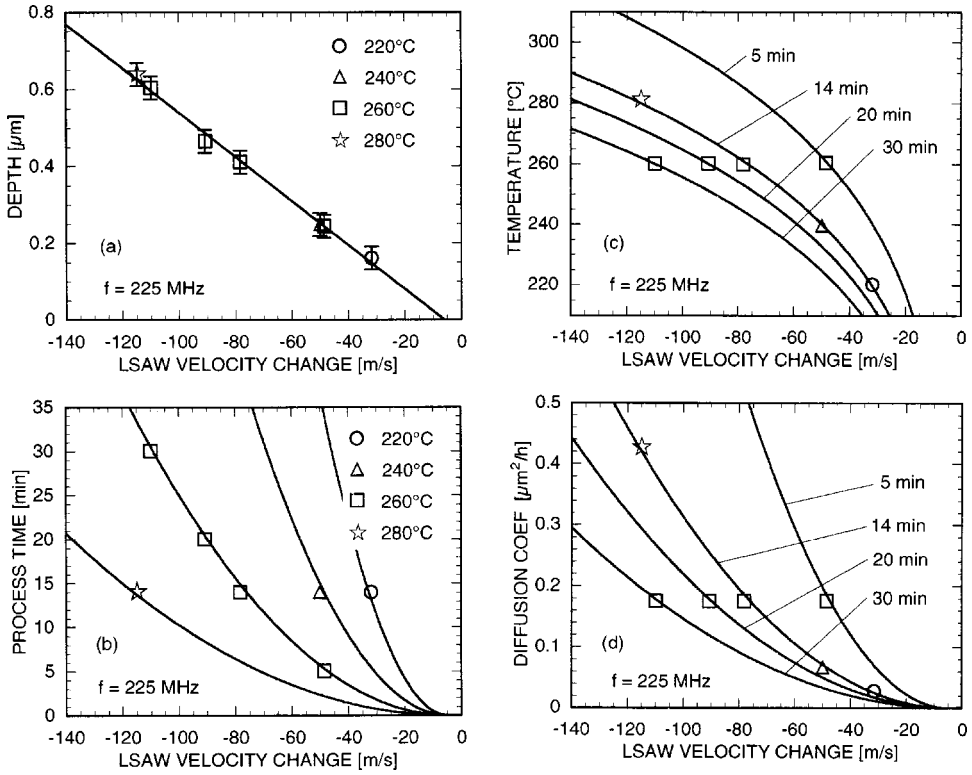

FIG. 7. Experimental relationships among LSAW velocities at 225 MHz, depths of proton-exchanged layers (a), process times (b), process temperatures (c), and diffusion coefficients (d) for proton-exchanged, *Z*-cut $LiTaO_3$ specimens.

B. Relationship between LSAW velocities and process conditions

The LSAW velocities obtained in Sec. IV can be related to the conditions of process time and temperature and the measured depths of proton-exchanged layers in Table I. Figure 7(a) shows the relationship between the LSAW velocity changes and the depths. Figures 7(b)–7(d) show the relations of the LSAW velocity changes with the process times, the process temperatures, and the diffusion coefficients. The LSAW velocity changes obtained for the *Y*-axis propagation at 225 MHz were used. The temperatures at which the specimens were prepared are indicated by circles (220 °C), triangles (240 °C), squares (260 °C), and stars (280 °C) in the figures. The solid straight line in Fig. 7(a) is the line approximated by the least-squares method, represented by the equation

$$H = -0.00574\Delta V_{\mathrm{LSAW}} - 0.0349, \tag{4}$$

where ΔV_{LSAW} is the LSAW velocity change. The relationships of the LSAW velocity change to the process time, process temperature, and diffusion coefficient are given by solving Eqs. (2) and (3) and using the relation:

$$\Delta V_{\mathrm{LSAW}} = -0.783fH - 4.72, \tag{5}$$

which is the approximated line by the least-squares method for all the measured fH dependences of LSAW velocity changes shown in Fig. 6. The solid lines in Figs. 7(b)–7(d) are the calculated results. The measured relationships between the LSAW velocity changes and each of the parameters agree well with the calculated results. The LSAW velocity decreases in proportion to the proton-exchanged layer depth as the process time increases and the process temperature increases. Table II shows the sensitivities and resolutions to the depth, fabrication process time and temperature, and diffusion coefficient. The resolutions were calculated corresponding to the resolution at an LSAW velocity of $\pm 0.002\%$ (± 0.1 m/s around 3300 m/s) measured at a single chosen point by the LFB system.[28] Therefore by measuring the LSAW velocity distributions at a single frequency and using the relationships given in Fig. 7, both depth distributions of the proton-exchanged layers formed on the surface and distributions of fabrication process conditions during proton exchange, which depend upon the fabrication process procedures and systems, can be evaluated with very high resolution.

C. Homogeneity in a 2-in. wafer

Homogeneity of a proton-exchanged, 2-in. *Z*-cut $LiTaO_3$ wafer was examined with the LFB-UMC system. As shown in Fig. 8(a), the $LiTaO_3$ wafer was proton exchanged in a 300-cm^3 beaker. The axes of the coordinates in the figure indicate the crystallographic axes of the specimen. The cross

TABLE II. Sensitivity and resolution for depth of a proton-exchanged layer and parameters of fabrication conditions during proton exchange by LSAW velocity measurements.

	Sensitivity	Resolution
LSAW velocity		± 0.1 m/s
Depth	5.7 nm/(m/s)	± 0.57 nm
Diffusion coefficient	4.9×10^{-3} (μm^2/h)/(m/s)	$\pm 0.49\times10^{-3}$ (μm^2/h)
Process time	6.55×10^{-3} h/(m/s) (23.6 s/(m/s))	$\pm 0.655\times10^{-3}$ h (± 2.4 s)
Process temperature	0.6 °C	± 0.06 °C

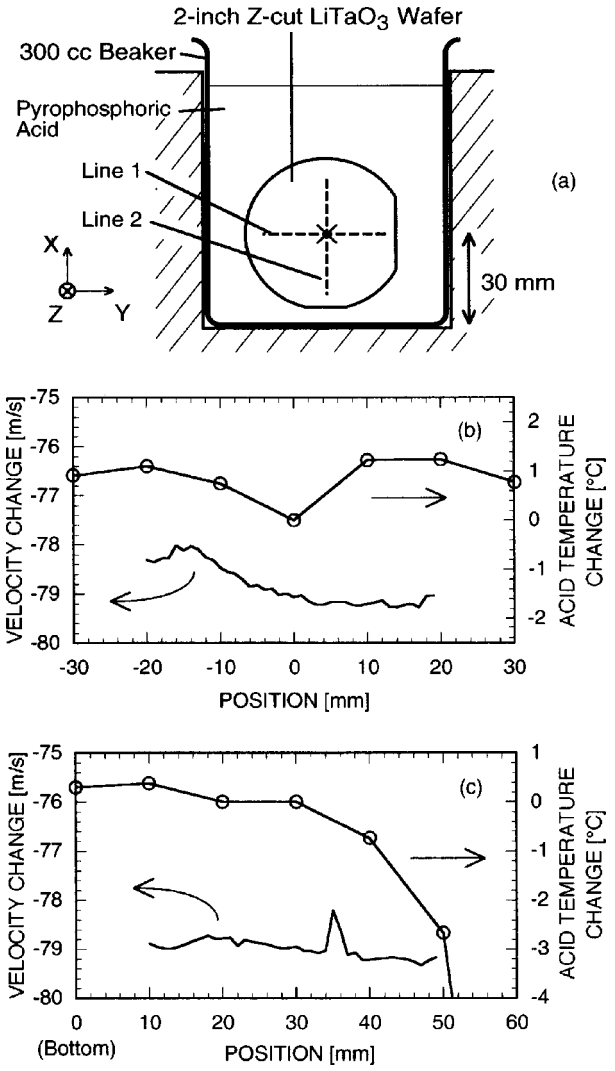

FIG. 8. Homogeneity evaluation of a proton-exchanged, 2-in. *Z*-cut $LiTaO_3$ wafer by LSAW velocity measurements. (a) Sample preparation. (b) Variations of LSAW velocities and acid temperatures along line 1, and (c) along line 2 shown in (a).

mark shows the center of the wafer. The wafer center was placed along the central axis of the beaker and 30 mm above the bottom, where the temperature distribution is nearly uniform. Proton exchange was carried out using the procedures described in Sec. III, except that a 300-cm^3 beaker was used for the proton exchange after preheating the wafer and sample holder up to the process temperature in the neighboring furnace hole for a 500-cm^3 beaker before the process. The temperature of the pyrophosphoric acid solution for the central position of the wafer was 260.5 °C and the process time was 14 min for fabricating optical waveguides. The proton exchange was successfully carried out without roughening or cracking the wafer. Figures 8(b) and 8(c) show the differences in the LSAW velocities before and after the process measured in 1-mm steps along lines 1 and 2 in Fig. 8(a), which are shown by the dotted lines. The measurements were conducted with the LSAWs propagating along the *Y*-axis direction at 225 MHz. The 0-mm position on the abscissa in Fig. 8(b) indicates the center of the wafer. The abscissa in Fig. 8(c) represents the distance from the bottom of the beaker. The LSAW velocity changes are the smallest around −15 mm along the diameter direction of the beaker, and slightly larger but nearly flat in the right side of the beaker, exhibiting a little asymmetry with respect to the central axis of the beaker. Only very small LSAW velocity changes were observed in the depth direction in Fig. 8(c), with an anomaly at the 35-mm position, where the LSAW velocity change was about 0.8 m/s, smaller than those at the other positions. These velocity changes are much larger than the measurement resolution of about 0.1 m/s, and the elastic properties at these points differ distinctively from those at the positions around them. Although it is understood that these changes were induced by the proton exchange, the direct cause has not been identified. This should be clarified soon because it could be an important problem in the device fabrication processes if the devices are to be manufactured. The distributions of the LSAW velocity changes are 1.3 m/s in Fig. 8(b) and 0.6 m/s in Fig. 8(c), except for the anomalies, which are seen from Table II to correspond to 7.4 and 3.4 nm in the depth variations, since it is understood from the results in the preceding section that the distributions of the LSAW velocity changes directly reflect the depth distributions of the proton-exchanged layers. This depth distribution might be mainly caused by the distribution of the diffusion coefficient due to the temperature distribution of the pyrophosphoric acid solution in the beaker. The process temperatures were estimated from the LSAW velocity changes using the results in Fig. 7. The temperature distributions are estimated to be 0.8 °C in Fig. 8(b), where the temperatures are lower in the left side and higher in the right side of the beaker, and 0.4 °C in Fig. 8(c), where the temperatures remain almost unchanged.

When the beaker contained only the pyrophosphoric acid solution, temperatures of the acid solution were measured with the thermocouple in 10-mm steps over lines 1 and 2 along which the LSAW velocities were measured. The differences from the acid temperature measured at the central position of the wafer are shown by circles in Figs. 8(b) and 8(c). In Fig. 8(b), the temperatures of the pyrophosphoric acid solution were higher in the outer regions than in the center along the beaker diameter direction, and a maximum temperature variation of 1.3 °C was observed. The temperature profile exhibits a little asymmetry, with a slight decrease on the left side of the beaker. In Fig. 8(c), the temperature of the pyrophosphoric acid decreases monotonically from the bottom to the surface, with a maximum temperature variation of 3.1 °C over the distance. The measured temperature profiles might differ somewhat from the true temperature distributions during the proton exchange because changes of ambience such as the liquid surface rising and the convection of the acid solution being physically and thermally disturbed when the 2-in. wafer and sample holder were immersed. However, the results clearly indicate some temperature variations in the proton-exchange process on the wafer surface.

In fabricating optical waveguides, waveguides with desired depths have to be manufactured precisely and uniformly for the light propagation modes depending upon the waveguide properties. According to an article by Yamamoto *et al.*,[29] a difference of 20 nm from the designed depth value

results in a 50% reduction in the intensity of second harmonics generated in a $LiTaO_3$ proton-exchanged optical waveguide for a QPM-SHG device because of mode dispersion. Therefore depth distributions of the waveguides to be fabricated must be much less than 20 nm over a whole surface for future mass production with large-diameter wafers. The LFB system has very high resolution as shown in Table II and can be used to evaluate large-diameter wafers in a short time as seen in Fig. 8. The LFB system is considered a very useful technique for evaluation and establishment of fabrication processes and systems for mass production.

VI. CONCLUSIONS

This article reports on an experimental investigation and discussions to obtain basic data and to establish experimental procedures required for applying the LFB-UMC system, operating in the frequency range of 100–300 MHz, to evaluate proton-exchanged optical waveguides prepared in a pyrophosphoric acid solution as well as their fabrication processes and systems. The process time and temperature were taken as typical parameters in the proton-exchange process, and LSAW velocity measurements, H and Li depth profile analyses by SIMS, and depth measurements of the proton-exchanged layers were conducted for proton-exchanged *Z*-cut $LiTaO_3$ specimens prepared with these parameters varied.

Angular dependences of LSAW velocities revealed that proton-exchanged *Z*-cut $LiTaO_3$ specimens should be characterized and evaluated in the *Y*-axis propagation direction in which the sensitivities of LSAW velocity changes to the process condition changes are highest. Results of fH dependences of LSAW velocities determined using the proton-exchanged layer depths obtained by SIMS suggested that the fH dependence of LSAW velocities for every specimen overlapped each other, exhibiting an almost constant change rate of -0.78 (m/s)/(Hz m) for pyrophosphoric acid as the proton source. In practice, H and Li depth profiles indicated that the elastic properties of proton-exchanged layers were not uniform in the depth direction and had some distributions based on the diffusion process. However, the above results in the fH dependences support the idea that we can use a simple measurement model of a single-layer specimen within the fH range used here to characterize proton-exchanged specimens by this LFB-UMC system. Furthermore, we experimentally obtained the relationships of LSAW velocities with the proton-exchanged layer depths, the process times, the process temperatures, and the diffusion coefficients, and demonstrated extremely high LSAW velocity resolutions for these parameters. Homogeneity of a 2-in. *Z*-cut $LiTaO_3$ wafer with the whole surface proton exchanged was investigated using these results. This investigation suggested that LSAW velocity distributions inform us of some variations in the fabrication process conditions during proton exchange that we would otherwise be unable to measure.

Many optical waveguides using either $LiNbO_3$ or $LiTaO_3$ substrates are fabricated with annealing after proton exchange in order to reduce the optical propagation loss. Therefore to successfully apply the LFB system to evaluate optical waveguides and their fabrication processes, we must collect further basic data of elastic properties in the optical waveguides after annealing related to other data of optical waveguide refractive indices and H and Li depth profiles.

ACKNOWLEDGMENTS

The authors would like to express their sincere gratitude to K. Yamamoto and K. Mizuuchi of Matsushita Electric Industrial Co., Ltd. for their helpful advice concerning the preparation of the specimens, to T. Sato of the Institute for Advanced Materials Processing, Tohoku University, for analyzing the specimens by SIMS, and to T. Okuzawa for constructing the fabrication system for proton exchange. This work was supported in part by a Research Grant-in-Aid from the Ministry of Education, Science and Culture of Japan.

[1] K. Noguchi, H. Miyazawa, and O. Mitomi, IEICE Trans. Electron. **E81-C**, 1316 (1998).
[2] H. Nakajima, IEICE Trans. Electron. **E82-C**, 297 (1999).
[3] H. Herrmann, K. Schäfer, and C. Schmidt, IEEE Photonics Technol. Lett. **10**, 120 (1998).
[4] K. Yamamoto, K. Mizuuchi, K. Takeshige, Y. Sasai, and T. Taniuchi, J. Appl. Phys. **70**, 1947 (1991).
[5] A. Grisard, E. Lallier, G. Garry, and P. Aubert, IEEE J. Quantum Electron. **33**, 1627 (1997).
[6] J. L. Jackel, C. E. Rice, and J. J. Veselka, Appl. Phys. Lett. **41**, 607 (1982).
[7] K. Nakamura and H. Shimizu, Appl. Phys. Lett. **56**, 1535 (1990).
[8] R. G. Wilson, S. W. Novak, J. M. Zavada, A. Loni, and R. M. De La Rue, J. Appl. Phys. **66**, 6055 (1989).
[9] P. K. Tien and R. Ulrich, J. Opt. Soc. Am. **60**, 1325 (1970).
[10] J. M. White and P. F. Heidrich, Appl. Opt. **15**, 151 (1976).
[11] D. F. Clark, A. C. G. Nutt, K. K. Wong, P. J. R. Laybourn, and R. M. De La Rue, J. Appl. Phys. **54**, 6218 (1983).
[12] J. Kushibiki and N. Chubachi, IEEE Trans. Sonics Ultrason. **SU-32**, 189 (1985).
[13] J. Kushibiki, T. Kobayashi, H. Ishiji, and C. K. Jen, J. Appl. Phys. **85**, 7863 (1999).
[14] J. Kushibiki, T. Okuzawa, J. Hirohashi, and Y. Ohashi, J. Appl. Phys. **87**, 4395 (2000).
[15] J. Kushibiki, T. Ishikawa, and N. Chubachi, Appl. Phys. Lett. **57**, 1967 (1990).
[16] J. Kushibiki, M. Miyashita, and N. Chubachi, IEEE Photonics Technol. Lett. **8**, 1516 (1996).
[17] J. Kushibiki and M. Miyashita, Jpn. J. Appl. Phys., Part 2 **36**, L959 (1997).
[18] A. Tourlog, J. D. Achenbach, and J. Kushibiki, J. Appl. Phys. **81**, 6616 (1997).
[19] P. J. Burnett, G. A. D. Briggs, S. M. Al-Shukri, J. F. Duffy, and R. M. De La Rue, J. Appl. Phys. **60**, 2517 (1986).
[20] K. Hano, N. Chubachi, and T. Sannomiya, Electron. Lett. **28**, 2306 (1992).
[21] J. Kushibiki and Y. Ono, IEEE Trans. Ultrason. Ferroelectr. Freq. Control (submitted).
[22] J. Kushibiki, Y. Ohashi, and M. Arakawa, IEEE Trans. Ultrason. Ferroelectr. Freq. Control **47**, 274 (2000).
[23] Y. Ohashi and J. Kushibiki, Jpn. J. Appl. Phys., Part 2 **38**, L1197 (1999).
[24] J. A. Armstrong, N. Bloembergen, J. Ducuing, and P. S. Pershan, Phys. Rev. **127**, 1918 (1962).
[25] K. Mizuuchi, K. Yamamoto, and H. Sato, J. Appl. Phys. **75**, 1311 (1994).
[26] E. M. Biebl, P. H. Russer, and K. Anemogiannis, *Proceedings of the IEEE Ultrasonics Symposium IEEE*, (New York, 1989), pp. 281–284.
[27] M. Hirabayashi, T. Yamasaki, and Y. Komatsu, Jpn. J. Appl. Phys., Part 1 **32**, 2355 (1993).
[28] J. Kushibiki and M. Arakawa, IEEE Trans. Ultrason. Ferroelectr. Freq. Control **45**, 421 (1998).
[29] K. Yamamoto, K. Mizuuchi, and T. Taniuchi, IEEE J. Quantum Electron. **28**, 1909 (1992).